CHAPTER 1

Quality of lossy compressed images and ways of its providing

Volodymyr Lukin
Sergii Kryvenko
Fangfang Li
Sergiy Abramov
Viktoriia Abramova
Bohdan Kovalenko
Igor Dohtiev
Oleksandr Arkhipov
Nenad Stojanović
Boban Bondžulić

Abstract

A task of lossy compression of images with providing a desired quality is considered. Image properties and metrics that are able to characterize compressed image quality including visual quality are briefly discussed. It is mentioned that a reasonable compromise between compression ratio and quality has to be provided in practice where a larger compression ratio usually leads to worse quality according to different criteria. Examples of basic dependencies are given and it is shown that the basic characteristics of compression considerably depend on image complexity that can be described by entropy or some other parameters. In addition, the compromise depends on a coder used and a parameter it employs for compression control. Analysis of basic rate-distortion curves is carried out and it is demonstrated that a desired quality according to a given metric is provided for a wide range of values of a parameter that controls compression (PCC) for a given coder. Then, the corresponding PCC has to be provided for a considered coder. Several ways to do this are considered. Drawbacks of setting a fixed PCC are discussed. A two-step approach is described and its basic properties are considered. Advantages and disadvantages of this approach are presented. An approach based on just noticeable difference is described. Its positive features and restrictions are presented. Finally, conclusions are given.

 DOI: 10.21303/978-9908-845-05-0.ch1

Keywords
Lossy compression, images, quality control, rate, distortion curve, accuracy.

1.1 Introduction

Lossy compression of images is currently widely employed in different applications including remote sensing [1], medical diagnostics [2], military [3], forestry and agriculture [4, 5], ecological monitoring [6], and so on. On one hand, images of different origin are able to provide useful information about sensed terrains, objects, and phenomena where imaging is a convenient way to have pre-requisites to obtain and retrieve such information from acquired data. On the other hand, average size of modern images and their number have an obvious tendency to increasing that makes problematic the image data transfer, storage, and dissemination. This stimulated the need in image compression where lossless compression, although being still used in some applications [7], becomes less popular [8]. The main reason is that lossy compression is able to provide a significantly larger compression ratio (CR) than for lossless compression (up to tens and hundreds [9]), that can be varied.

Meanwhile, lossy compression leads to distortions (losses, degradations) that can have different level and properties depending on many factors [9–13]. The main of them are complexity of an image subject to compression [10, 11, 13], a used compression technique and a value of a PCC [9, 13] (e.g., quality factor (QF) serves as PCC in JPEG), noise presence or absence [12], etc. A general tendency is that the introduced losses increase and a compressed image quality diminishes if CR becomes larger (although there are specific exceptions relating to the so-called strange images [14]). Then, a question arises what is an appropriate compromise between CR and image quality [8, 9, 15–17]? An answer to this question depends on a goal a compressed image is used. A compressed image can be a subject for visualization to perceive or analyze it. Then, visual quality is of prime importance and visually lossless compression can be helpful [9, 17, 18]. A compressed image can be also employed for classification or recognition [4, 19, 20]. Then, a task is to prevent significant (inappropriate) degradation of classification and object recognition accuracy due to lossy compression.

The next question is how this compromise can be attained in practice. An answer to it again depends on a coder used, chosen approach or metric to characterize compressed image quality, noise presence or absence, image complexity, and requirements to accuracy to image quality providing and computational complexity [9–13]. The size of an image to be compressed and a number of channels (components)

in this image might have an impact too. Therefore, a plethora of studies has to be carried out or the results under interest have to be retrieved from different papers to answer these questions. Below, let's present some results described in our recent papers as well as consider the outcomes and conclusions from the papers of other authors to give an insight on theoretical and practical solutions available for providing a desired quality of lossy compressed images.

1.2 Considered images and their properties

Images employed in different applications might be acquired by different types of sensors and, thus, their main properties (size, number of components, complexity, noisy or not) can vary within wide limits. Images containing millions of pixels can be met in practice of remote sensing, medical diagnostics, and customer digital photos very often. Whilst single- (e.g., medical or synthetic aperture radar) and three-channel (e.g., color) images are, probably, the most common, two-channel (dual-polarization) data and images with about ten (multispectral) and even hundreds (hyperspectral) of components are good candidates for lossy compression, too. In the latter two cases, the image size can be especially large [8, 21, 22].

Concerning image complexity, different approaches to describe it are possible. In particular, image entropy and many other parameters are able to reflect complexity of practically noise-free images [12, 23–26]. For example, **Table 1.1** presents four grayscale images of different complexity characterized by entropy E (the smaller, the simpler the image structure) and mean square error (MSE) values for distortions introduced by a better portable graphics (BPG) coder [27] for which Q (an integer-valued parameter from 0 to 51) serves as PCC where a larger Q corresponds to greater distortions and a larger CR. For smaller entropy, a smaller MSE is observed where for both values of Q the introduced distortions are invisible (this happens if distortions are similar to additive white Gaussian noise (AWGN) [11] and its variance is less than 20 for 8-bit grayscale images).

For noisy images, i.e. images for which noise is visible, the situation with characterizing their complexity is more complicated [23]. Many parameters applicable for characterization of complexity for noise-free images are sensitive to noise. Due to this, only a limited number of parameters able to do this exists. One of them is the percentage of pixels belonging to homogeneous image regions [26]. Meanwhile, noise type and characteristics might influence the estimates of this parameter. Recently, it has been shown that CR obtained for large degrees of image lossy compression might be good indicators of image complexity. To prove this, **Fig. 1.1** shows

dependencies of CR for compression of five typical test color image contaminated by AWGN with two values of the noise variance by the aforementioned BPG coder (mode 4:4:4) (noise is independent in image components). As seen, compression is practically near-lossless for $Q < 29$ (**Fig. 1.1, *a***) and $Q < 33$ (**Fig. 1.1, *b***) due to the influence of the noise for all images. Then, for larger Q, CR starts to grow quickly and for $Q \approx 45$ reaches tens and hundreds depending on image complexity irrespectively to noise variance. CR is the largest for the image Frisco ($E = 5.8$) and is the smallest for highly textural (complex structure) image Baboon ($E = 7.36$). Thus, it seems that CR for fixed PCC corresponding to large degree of compression might serve as an indicator of complexity of noisy images although this should be checked for different models of the noise that might be present in images subject to lossy compression. It is possible to note that similar effects have been observed in compressing grayscale images [27] (see **Fig. 1.2, *a***, the dependence is presented in logarithmic scale) and for the color images using BPG coder (mode 4:2:2, **Fig. 1.2, *b***).

Table 1.1 Four test grayscale images and entropy and MSE values for them ($Q = 20$ and $Q = 25$)

Test image 1 (Legs)	Test image 2 (Fr01)	Test image 3 (Fr02)	Test image 4 (Frisco)
		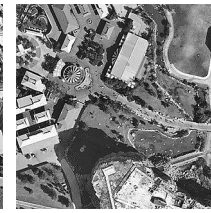	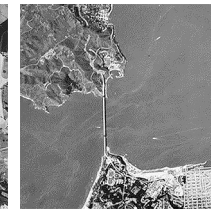
$Q = 20$			
$E = 6.50$	$E = 7.46$	$E = 7.40$	$E = 5.82$
MSE = 1.76	MSE = 1.90	MSE = 1.85	MSE = 1.17
$Q = 25$			
MSE = 4.57	MSE = 6.02	MSE = 5.78	MSE = 2.57

Below, let's mainly concentrate on images supposed noise-free. In fact, noise is present in practically all real-life images. However, it is possible to assume an image to be noise-free if noise is invisible. Noise invisibility takes place under certain conditions, e.g., is an image fully textural or has relatively large quasi-homogeneous regions. The fact is that texture masks noise, hence the noise can be noticed in quasi-homogeneous regions if it is intensive enough. For pure additive noise, it can be visible in 8-bit images for white noise if its variance exceeds 20–25 and for spatially

correlated noise if its variance exceeds 6–10. Thus, it is possible to assume an image noise-free if the noise is less intensive than the aforementioned thresholds.

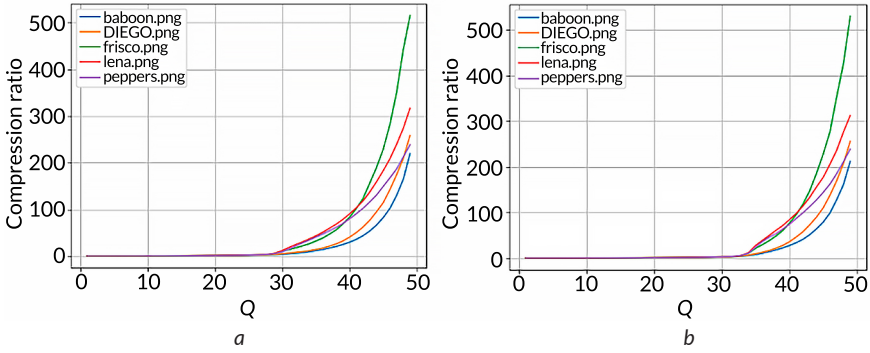

Fig. 1.1 Dependencies of CR on Q for five noisy color images for noise variance equal to 64 (*a*) and 196 (*b*)

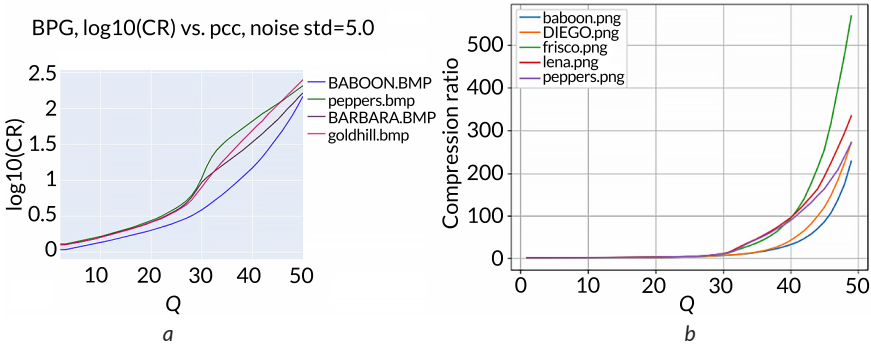

Fig. 1.2 Dependencies of CR on Q for four grayscale images for noise variance equal to 25 (*a*) and five color images for noise variance equal to 100 (*b*) for the BPG coder

Fig. 1.3 gives an example. The test grayscale image Fr03 is corrupted by AWGN with noise variance equal to 25. This noise can be hardly noticed in quasi-homogeneous region in the central part of this image. Meanwhile, the noise is invisible in textural regions, e.g., in the left lower corner of this image, due to the masking effect of texture. This image as well as two images (Fr01 and Fr02) in the central part of **Table 1.1** can be treated as typical examples of images acquired by sensors installed on-board of unmanned aerial vehicles (UAVs) and drones.

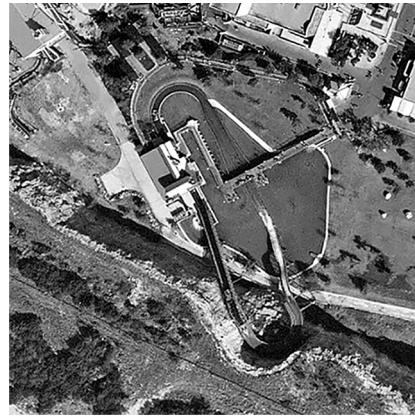

Fig. 1.3 An example of noisy image with hardly noticeable additive white Gaussian noise

Note that, with gaining the popularity of using such sensors, there is practically no difference nowadays between images obtained by remote sensing means (i.e., acquired from some airborne carrier) and standard customer cameras (for some landscapes or urban areas from windows or balconies of multi-store buildings).

1.3 Considered metrics and their properties

If to deal with lossy compression, the introduced distortions have to be characterized quantitatively. For many years, MSE and peak signal-to-noise ratio (PSNR), for single-channel 8-bit image it is determined as PSNR = $10 \log_{10}(255^2/\text{MSE})$ have been the most widely used. In fact, they are still widely used, but the tendency for using visual quality metrics becomes more obvious. There are several reasons behind this. First, as mentioned above, (compressed) images are most often subject to visual inspection and analysis [28–31]. Second, the theory of visual quality metrics has greatly advanced [32–34] in recent 30 years starting from the discrete cosine transform (DCT) based metric DCTune [35] and completing with modern neural network based metrics [36] whilst problems of PSNR in reliable assessment of image visual quality have been shown many times. Third, there is correlation between classification accuracy and both traditional (such as PSNR) and visual quality metrics where the latter ones better correlate with classification accuracy for such "heterogeneous" classes as "Urban" or "Vegetation" in opposite to "homogeneous" classes as "Water surface" or "Grass" [37].

The problems of PSNR can be shown for visually lossless compression that can be also treated as determination of just noticeable difference (JND) point No. 1, i.e. minimal distortions that can be noticed by observers. For example, for the most known coder (standard) JPEG, quality factor (QF) is employed as PCC where QF is integer from 1 to 100 and 100 corresponds to perfect quality (practical absence of distortions). According to data in [9], JND No. 1 for different images takes place for PSNR in the limits from 23 dB to 43 dB and for QF in the limits from 31 to 79. This means the following. First, if one sets PSNR = 43 dB or QF = 79 to guarantee that invisibility of distortions is provided, then for a large percentage of images there is a large space to set a smaller PSNR or QF in order to have a larger CR with still invisible distortions. Second, JND No. 1 is very individual and depends on image complexity.

According to the visual quality metric PSNR-HVS-M [38] (HVS relates to human vision system and M relates to masking) also expressed in dB, the limits of its variation are narrower – from 37.5 dB to 50.5 dB. Thus, it is more adequate but is still not perfect. The situation is similar for some other visual quality metrics [39].

It is difficult to say how many visual quality metrics have been proposed so far. Meanwhile, it is clear that their number exceeds 150 and continues to grow each year. There are several reasons for such a large number of visual quality metrics and attempts to design new ones. First, even the best visual quality metrics are not perfect (this especially relates to no-reference metrics). Second, there is a desire to design universal visual quality metrics [40], i.e. such metrics that are adequate enough for a wide set of distortion types (e.g., there are 24 types of distortions in the database TID2013 [41], here TID2013 relates to Tampere International Database created in 2013). This is a hard task since it is difficult to take into account all peculiarities of human vision system (HVS) and its reaction to specific features of various distortions. The attempts to make this on basis of neural networks that either combine a set of features extracted from an image to be compressed [36, 42] or a set of good visual quality metrics [40, 43, 44] lead to the better universality by the expense of more computations (and time) needed for the metric calculation. Meanwhile, the needed computation time (expanses) is often an important characteristic of a visual quality metric determining its use in practice [45].

While efforts to design better universal metrics continue, a more specific direction of research is to find proper metrics for a particular application such as lossy compression of images in our case. In this sense, the obtained achievements are more obvious. But before starting to consider them, it is necessary to recall how visual quality metrics are compared and analyzed. Usually, image databases with different types of distortions and available assessments (estimates) of image visual quality presented as mean opinion score (MOS) are employed for this purpose. A good visual quality

metric should have a high (at least, rank) correlation between its values and MOS for one or several databases containing images with distortions of interest (saying "high", let's mean that Spearman rank order correlation coefficient (SROCC) has to approach either 1 or –1; the former holds for most metrics that have larger values for better quality, the latter relates to some metrics that have smaller values for better quality such as MSE and Mean Deviation Similarity Index (MDSI) [46]).

Analysis of references dealing with analysis and comparison of metric properties shows the following. Whilst most metrics have SROCC not exceeding 0.9 for all types of distortions in the database TID2013 [43], there are several metrics that have SROCC exceeding 0.92 for the most important distortion types aggregated in subsets "Noise" and "Actual" that correspond to different types of the noise and denoising and lossy compression applications. Recall that PSNR and widely used structural similarity index measure (SSIM) have SROCC values for these subsets smaller than 0.83 and 0.79, respectively.

Moreover, if one considers only distortions dealing with lossy compression, SROCC reaches 0.96–0.97 for such metrics as PSNR-HVS-M [38], MDSI [46], HaarPSI (Haar wavelet-based perceptual similarity index) [47], FSIM (Feature Similarity Index) [48], and some others. Let's note that codes for calculation of aforementioned metrics are available for PSNR-HVS-M, and in Python for MDSI, for HaarPSI, and for FSIM.

Furthermore, there is a very high correlation between the best visual quality metrics [49]. For example, SROCC between MDSI and PSNR-HVS-M is larger than 0.96, between MDSI and HaarPSI – larger than 0.97, between MDSI and FSIM – larger than 0.98 (other data can be found in [49]). And this is not surprising since metrics that have high correlation with MOS should have high correlation between each other. Moreover, good metrics can be recalculated to each other [45]. To show this, **Fig. 1.4** shows the scatter-plot PSNR-HVS-M vs HaarPSI for images with three types of distortions dealing with lossy compression in TID2013. The following expression is valid

$$HaarPSI = -0.0005338 \times PSNR\text{-}HVS\text{-}M^2 + 0.053923 \times PSNR\text{-}HVS\text{-}M - 0.3612, \quad (1.1)$$

where goodness-of-the-fit indicator $R^2 = 0.977$, i.e. is very large.

This means that, for characterizing visual quality of lossy compressed images, one can use any of aforementioned metrics as well as some other good metrics mentioned in [49]. While choosing them for a particular application or analysis, the following properties can be taken into account:

1) experience of working with a given metric including knowledge on approximate positions of JND No. 1 and other JND points;

2) linearity of dependencies of a metric on PCC for a given coder and on MOS for a given database;

3) computational efficiency of metric calculation, etc.

The importance of these properties will become clear later.

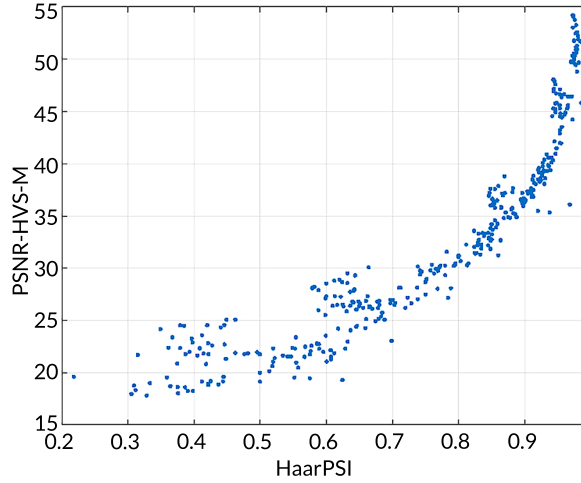

Fig. 1.4 The scatter-plot of PSNR-HVS-M vs HaarPSI for images with three types of distortions dealing with lossy compression in TID2013

Summarizing the brief analysis of metrics able to characterize quality of compressed images, it is possible to state the following. There are several visual quality metrics that are, certainly, not perfect but able to describe quality of lossy compressed images very adequately. To avoid arguments that some compression techniques are based on DCT and a used metric is also based on DCT (similarly for coders based on wavelets and metrics employing wavelets), it is possible to recommend using joint analysis of two metrics based on different transforms or principles of their calculation in studying the performance of lossy compression approaches.

1.4 Some analyzed coders

It is impossible to consider all existing methods of lossy compression. Because of this, let's further rely on data obtained for several typical representatives of compression techniques based on orthogonal transforms since just wavelets and

DCT serve as the basis of most modern practically used coders employed for lossy compression of images and video. The main advantage of this group of methods is that they are quite efficient in different senses – providing quite high quality and ease of variation of compression parameters (CR and quality). Alongside with JPEG, QF is also applied in AV1 Image File Format (AVIF) and High Efficiency Image File Format (HEIF) coders [50, 51]. Bits per pixel (BPP) serves as PCC for JPEG2000 [52] and Set partitioning in hierarchical trees (SPIHT) [53] coders, quantization step (QS) is used in DCT-based coders AGU [54] and advanced DCT (ADCT) [55] coders, scaling factor (SF) serves as PCC in visual quality oriented versions of AGU and ADCT [13] (AGU-M and ADCT-M where M relates to Modified), parameter Q is applied in the BPG coder [27].

Some aspects of using these PCCs will become clear below. They are quite different. JPEG2000 is oriented on easy providing a desired CR, others are more intended on providing a desired quality although, as mentioned above, there are problems with establishing a direct dependence between a PCC and compressed image quality. Let's demonstrate this by two examples. **Fig. 1.5** shows the values of PSNR-HVS-M for the coder AGU-M for two values of BPP – 0.75 (CR = 10.5) and 1.6 (CR = 5).

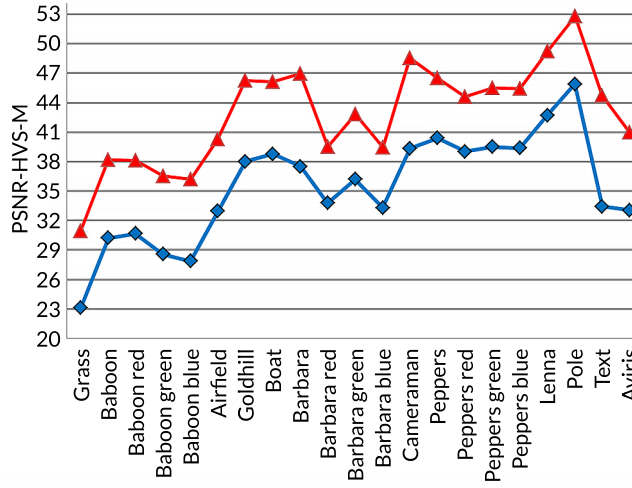

Fig. 1.5 PSNR-HVS-M for several grayscale (component) images compressed by AGU-M with providing two values of BPP, 0.75 (blue color) and 1.6 (red color)

The metric is calculated for images of different origin: conventional grayscale test images, component images of conventional test color images, simple and complex structure test images Pole and Grass, respectively, component image of

AVIRIS (Airborne Visible/InfraRed Imaging Spectrometer) hyperspectral data. As expected, PSNR-HVS-M for BPP = 1.6 is always larger than for BPP = 0.75. Meanwhile, in both cases, PSNR-HVS-M varies in very wide limits – from 23 dB to 46 dB for BPP = 0.75 and from 30 dB to 53 dB for BPP = 1.6. Keeping in mind that PSNR-HVS-M for JND No. 1 is from 37.5 dB to 50.5 dB, it occurs that for some images the distortions are invisible for sure, for some other images it is guaranteed that they are visible whilst for many images (especially for BPP = 1.6) the visibility of distortions is of question. There is also one more observation. The metric values for component images of the same color image (e.g., Barbara) are very close. Let's recall that component images for a given color image are usually highly correlated [56], i.e., similar to each other, and, thus, images of similar complexity are compressed with providing similar quality. It is also seen that if CR increases (BPP decreases) by about 2 times, PSNR-HVS-M diminishes by about 7 dB.

One important question that usually arises in lossy compression is what coder to use? Although there are numerous papers and books showing advantages of newly designed lossy compression techniques, the answer is not simple. A really good coder should outperform its counterparts for different images, different compression ratios, and according to different criteria (metrics). However, this does not hold for any existing coder. **Fig. 1.6** presents dependencies of PSNR-HVS-M on CR for several known and modern compression techniques.

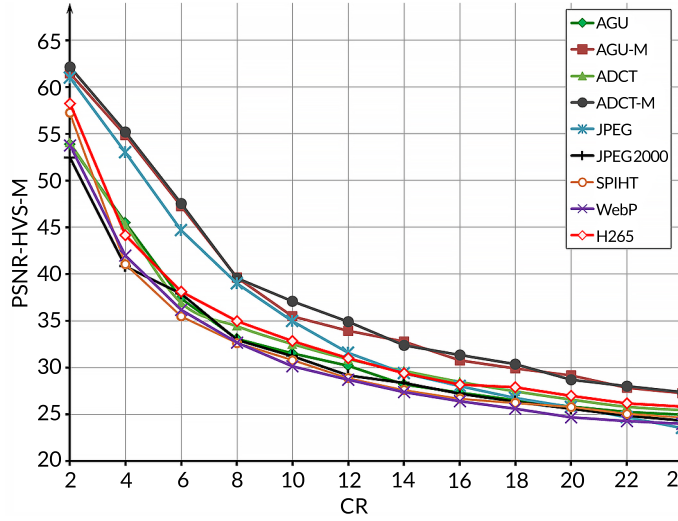

Fig. 1.6 PSNR-HVS-M vs CR for different coders applied to grayscale image Baboon

For *CR* ≈ 4, distortions are invisible for JPEG, ADCT-M, and AGU-M, i.e. coders "adjusted" to peculiarities of HVS by using specific quantization tables for DCT coefficients. For CR ≈ 6 and 8, advantages of these coders compared to other ones remain obvious where distortions are, most probably, visible for CR ≈ 8 for JPEG2000, WebP, AGU, ADCT, H.265, and SPIHT. For CR > 12, JPEG starts to be less efficient than AGU-M and ADCT-M but it performs practically at the same level as other coders. The main reasons behind these observations are that Baboon is a highly textural image and some coders (e.g., H.265 or JPEG2000) are more oriented on larger PSNR than better visual quality.

It might seem that data in **Fig. 1.6** are a particular example. However, there are other data showing that modern coders can perform worse than JPEG for a range of practical situations. For example, for visually lossless compression in JND No. 1 neighborhood, the BPG coder provides twice larger CR on the average than JPEG but the situations when CR for the BPG coder is slightly smaller than for JPEG for the same visual quality are also possible for particular images that usually have complex (textural) structure. In this case, the block size 8 × 8 pixels used in JPEG seems to be the optimal or quasi-optimal solution.

1.5 Rate/distortion curves and their properties

Fig. 1.6 presents an example of the so-called rate/distortion curves (RDCs) that are widely used in coder performance analysis and comparisons. In general, coders performance can be compared in different ways. One of them is to fix CR (or BPP) for all analyzed coders and compare the considered metric values. Another approach presumes fixing the quality metric and compare the CR values where then it is supposed that the best is the coder producing the largest CR. However, even the data in **Fig. 1.6** show the shortcomings of these approaches. Really, JPEG is among the best for CR = 4 whilst it is among the worst for CR = 24. In fact, the best coder should provide the best metric values for a wide (practically important) limits of CR variation, for all images, and for many metrics including PSNR and the best visual quality metrics. According to our experience, this never happens. Even if a coder demonstrates very good results for many images, it always happens that an image can be found for which this coder is not the best. For example, animation or drawings images are very specific. In addition, some coders are designed (optimized) to provide high performance according to PSNR, but then such coders can be not the best according to human vision system (HVS) metrics and vice versa.

Rate/distortion curves can be also used for analysis of compression characteristics depending on image (or image and noise) characteristics. Let's present and consider some examples. They are given in **Fig. 1.7** and **1.8**. Dependencies of PSNR and PSNR-based metrics on quantization step for the AGU and ADCT coders are presented in **Fig. 1.7** for a set of grayscale test images.

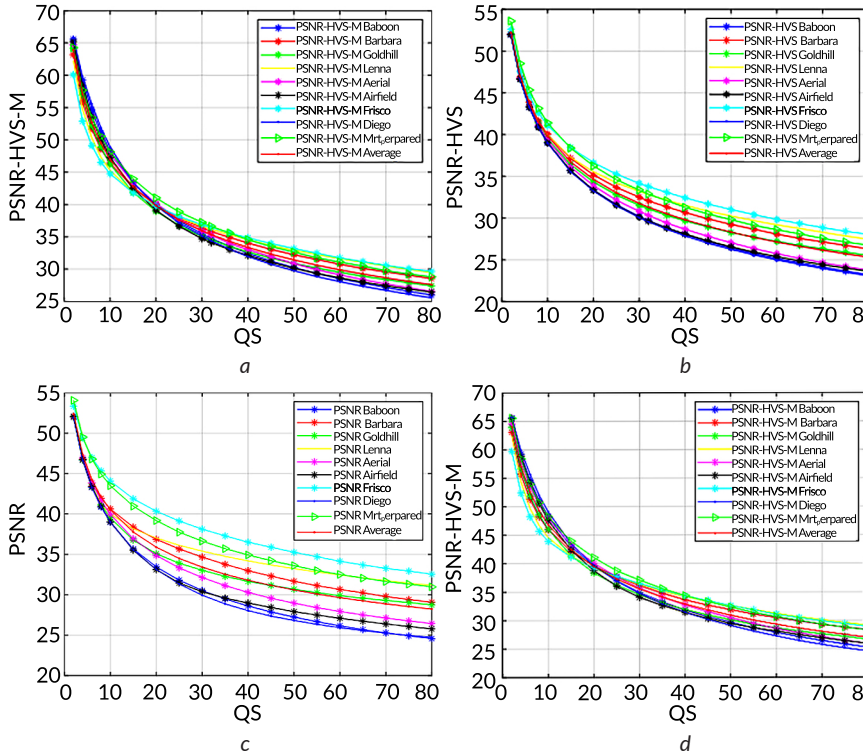

Fig. 1.7 Rate distortion curves for particular test grayscale images: *a* – PSNR-HVS-M(QS) for the AGU coder; *b* – PSNR-HVS(QS) for the AGU coder; *c* – PSNR(QS) for the ADCT coder; *d* – PSNR-HVS-M(QS) for the ADCT coder

The main observations are the following. First, all dependencies are monotonously decreasing. Second, most of them do not cross each other. In other words, if quality (according to a considered metric) of image1 is better than quality of image2 for QS_1, then, most probably, the same holds for other QS. Third, for QS > 20, quality of compressed simple structure images (such as Frisco and MRTprepared) is higher

than quality of complex structure images (Baboon, Diego). Thus, again there is the dependence of compression performance on image complexity. Fourth, locally, it can be assumed that individual dependencies are almost parallel to each other. In other words, for a given QS, they have almost the same derivative *dMetr/dQS* approximately equal to $(dMetr/dQS)_{av}$ obtained for average RDC (such RDCs are given in all four plots) where *Metr* is a considered metric. Moreover, there are intervals of QS (e.g., from 30 to 60) for which the dependencies are almost linear. These properties latter will be further used for quality providing.

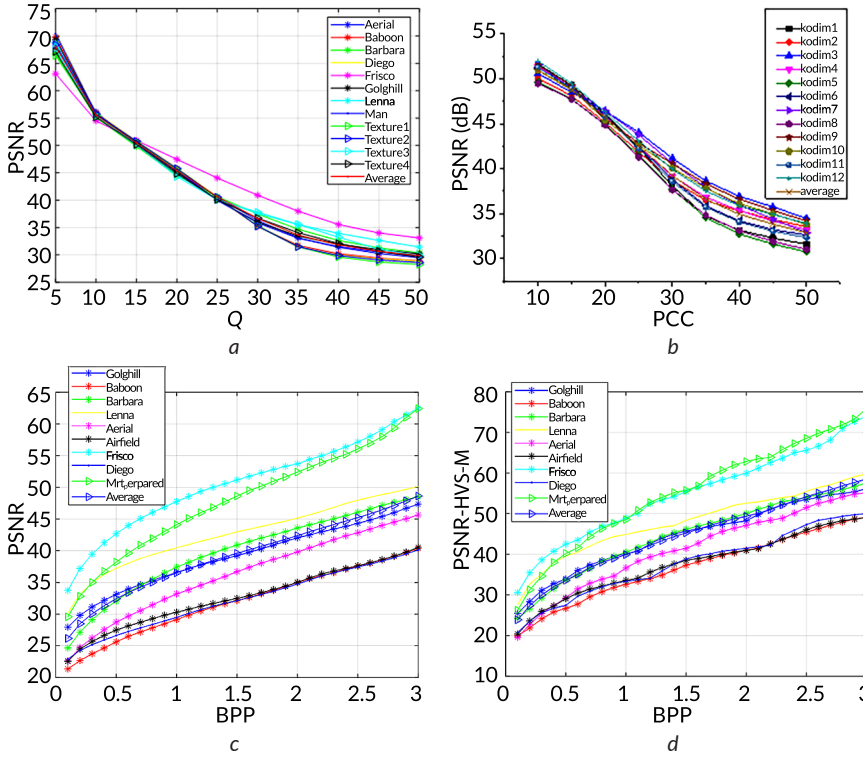

Fig. 1.8 Rate distortion curves for particular test images: *a* – PSNR(*Q*) for grayscale images compressed by the BPG coder; *b* – PSNR(*Q*) for color images compressed by the BPG coder; *c* – PSNR(BPP) for SPIHT; *d* – PSNR-HVS-M(BPP) for SPIHT

Analysis of data in **Fig. 1.8** shows the following. The RDCs PSNR(*Q*) for grayscale images behave in a compact way where only for the test image Frisco the RDC slightly

differs from others. In addition, the dependencies behave almost linearly for a wide range of Q that is of the main interest (from 10 to 35, i.e. from near-lossless to visually lossless compression). Analysis for color images (**Fig. 1.8, *b***) shows that the difference in PSNR for the same Q can be up to 5 dB but there is almost linear (and almost parallel) behavior of RDCs for a wide range of Q variation.

On the contrary, RDCs for SPIHT (**Fig. 1.8, *c, d***) have other properties. One reason is that these are dependent on BPP. The best quality according to both PSNR and PSNR-HVS-M is observed for the simple structure images Frisco and MRT prepared where the worst quality takes place for the complex structure image Baboon. The main problems for SPIHT and the corresponding RDCs for it are the following. First, for the same BPP, quality differs a lot. For example, PSNR values for $1 < \text{BPP} < 2$ differ by almost 20 dB. The same holds for the metric PSNR-HVS-M. Second, the derivatives of the metric on BPP are positive and they differ for particular images more than for previously considered RDCs. Although monotonous, the curves PSNR-HVS-M(BPP) have specific "variations".

1.6 Ways of providing a desired quality

First of all, let's explain what can be a desired quality of lossy compressed images. One option is that we would like to provide visually lossless compression. Another option is that, under assumption that a given visual quality metric is able to adequately characterize the image quality, we would like to provide a desired value of a chosen metric. These options might coincide in ways of reaching them but they are not the same. Let's start from the latter option since it can be a part of solving the former task.

Let's recall that it is possible to expect that a chosen metric is in good agreement with subjective estimates of image quality characterized by MOS. MOS values have different scales for different image databases used for image quality assessment. For example, in TID2013, MOS can be potentially from 0 to 9, but, in fact, the minimal value is about 0.2 and the maximal value is 7.2. In the paper [39], it was proposed to divide 3000 distorted images into four groups:

1) images having excellent quality (distortions are invisible or visual quality is considered to be very high); these are images having 200 top rank MOS values;

2) images having good quality; MOS for them have the ranks from 201 to 1000;

3) images of middle quality; for them, MOS have ranks from 1001 to 2000;

4) images of bad quality with the lowest 1000 ranks (from 2001 to 3000).

Note that ranking is carried out in the order of descending MOS. Quantitatively, the images of the first group have MOS larger than 6.05. For the second group,

MOS is in the limits from 5.25 to 6.05. MOS for the third group images is from 3.94 to 5.25. Finally, for the fourth group images, MOS is less than 3.94. This allows determining the thresholds for visual quality metrics using the corresponding scatter-plots and metric value ranking. An example is presented in **Fig. 1.9**. Processing of the obtained data shows that the image quality can be considered as excellent or good if HaarPSI exceeds 0.91. Meanwhile, image quality can be treated as bad if HaarPSI is smaller than 0.75. Similar conclusions can be drawn from analysis of data in **Fig. 1.10** where the scatter-plot of MOS vs HaarPSI is presented only for three types of distortions in TID2013 dealing with lossy compression. The results given in [45] show that invisibility of distortions is provided if HaarPSI exceeds 0.95 or, equivalently, if PSNR-HVS-M is larger than 41 dB (see data in **Fig. 1.4**).

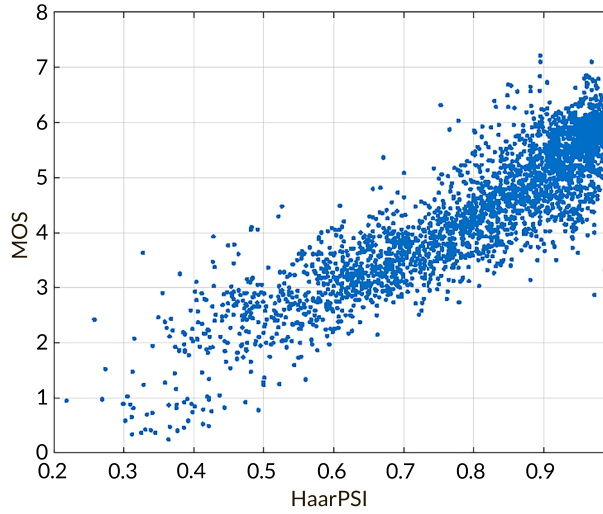

Fig. 1.9 The scatter-plot of MOS vs HaarPSI for all types of distortions in TID2013

It is possible to suppose now that we have decided to characterize image quality by HaarPSI or PSNR-HVS-M equal to 0.91 and 37.5 dB, respectively. It is also possible to assume that we have succeeded to provide them with very high accuracy. This means that MOS varies from approximately 5.2 to 6.0 (**Fig. 1.10**) that corresponds to good quality of compressed images (see above). In turn, MOS equal to 5.6 (the middle of the aforementioned interval) corresponds to HaarPSI from about 0.83 to 0.98 (**Fig. 1.10**). Then, there is no need to provide a desired value of a used metric $Metr_{des}$ with very high accuracy. For example, if $HaarPSI_{des}$ is provided

with errors smaller than 0.01 or the error of providing *PSNR-HVS-M*$_{des}$ is less than 1 dB, this can be treated as acceptable. Detailed analysis has shown that if a given image is compressed by a given coder with two values of PSNR-HVS-M differing from each other by less than 1 dB, they are mostly treated as having equal quality (and often treated as identical).

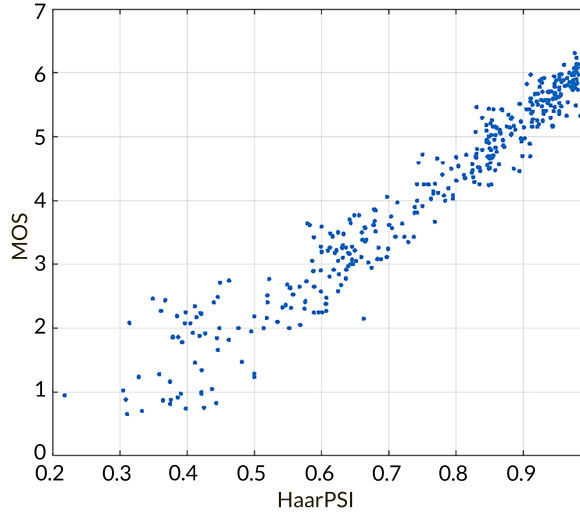

Fig. 1.10 The scatter-plots of MOS vs HaarPSI for three types of distortions dealing with lossy compression in TID2013

Let's now consider the methods of providing a desired quality by reaching some *Metr*$_{des}$. It is possible to start from iterative procedures mentioned above [13, 57, 58]. These methods imply image multiple compression/decompression, metric calculation, and changing PCC to approach *Metr*$_{des}$ with preset accuracy controlled after each iteration. The method performance depends on several factors. First, the starting point (initial value of a used PCC) plays an important role. A way the PCC is changed is important too. At the beginning, PCC can be changed with some discrete step, e.g., ΔQS for AGU or ADCT coders can be set equal to 2. When approaching to vicinity of *Metr*$_{des}$, it is possible to decrease the step of PCC changing or to apply linear interpolation (extrapolation) between the last two values *Metr*(*k*) and *Metr*(*k*–1) where *k* denotes the iteration index. The present accuracy of reaching *Metr*$_{des}$ might have influence too. Finally, for PCC having only integer values (such as QF for JPEG or Q for the BPG coder), it can be also so that it is impossible to ensure the desired accuracy

of reaching $Metr_{des}$ less than a certain limit. As it follows from data in **Fig 1.8, *a*, *b***, PSNR decreases by about 1 dB if Q increases by unity for the BPG coder. This means that it is principally impossible to provide $PSNR_{des}$ with error less than 0.5 dB. Some restrictions on accuracy of providing $HaarPSI_{des}$ for this coder are also studied in [45].

Thus, the number of iterations is unpredictable in advance and can be large enough. The results in [13, 57, 58] show that the number of iterations can be up to 10. This can cause problems if there are restrictions on compression time and/or if the compression/decompression time for a given coder is larger. For example, this happens for the ADCT coder for which compression takes certain time due to necessity to optimize partition schemes (decompression is faster). The number of iterations can be decreased for particular coders based on a priori knowledge concerning their main properties [13, 58]. In particular, average curves have been presented in [13] (**Fig. 1.11**) that allow setting the starting *QS* for AGU and ADCT coders (**Fig. 1.11, *a***) and *SF* for AGU-M and ADCT-M coders (**Fig. 1.11, *b***) to provide $PSNR\text{-}HVS\text{-}M_{des}$. The data in **Fig. 1.11, *a*** are in good agreement with data in **Fig. 1.6, *a*** although they have been obtained for different sets of test images. Due to better setting the starting point, it has occurred to decrease the number of iterations by 1.5–3 times [13, 58] with the same accuracy of providing $PSNR_{des}$ and $PSNR\text{-}HVS\text{-}M_{des}$. Moreover, sometimes, it is enough to have only one iteration. However, there are still practical situations where the corresponding computation time can be still inappropriate due to necessity to carry out, e.g., four iterations.

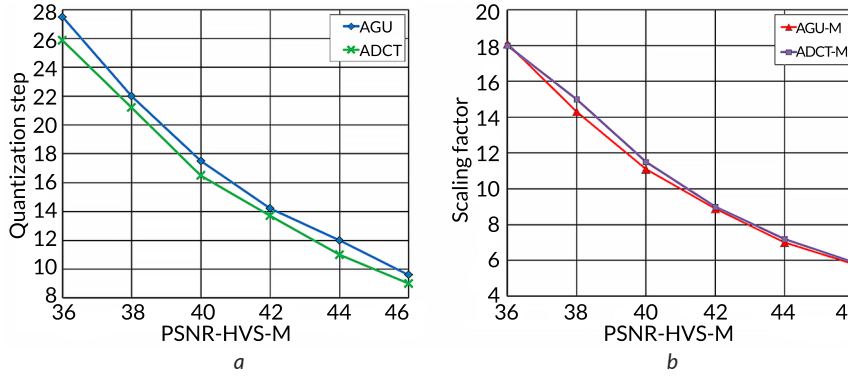

Fig. 1.11 Average curves of QS (*a*) and *SF* (*b*) on PSNR-HVS-M for AGU (*a*), ADCT (*a*), AGU-M (*b*), and ADCT-M (*b*) coders

It might seem that the obtained average curves can be used for setting fixed PCC that corresponds to $Metr_{des}$ for the average curve. This way of providing $Metr_{des}$ is very

fast but it is not accurate. Let's give a few examples to prove this. Suppose that one needs to provide $PSNR_{des}$ = 35 dB for the ADCT coder (see **Fig. 1.7, *c***). Then, one has to set QS ≈ 29. However, depending on an image to be compressed, the provided PSNR values are within the interval 30–38.5 dB, i.e. the errors obviously exceed 1 dB. The situation is slightly better for providing *PSNR-HVS-*M_{des} for the AGU (**Fig. 1.7, *a***) or ADCT (**Fig. 1.7, *d***) coders. Suppose *PSNR-HVS-*M_{des} equals to 35 or 40 dB. In this case, errors are less than 2 dB but, anyway, larger than 1 dB. Similar results have been obtained for 512 × 512 pixel fragments of medical images [59].

The situation is even worse for SPIHT and JPEG2000 (**Fig. 1.8**). Suppose $PSNR_{des}$ = 35 dB. Then, one has to set *BPP* = 0.8 (**Fig. 1.8, *a***). But then the provided PSNR is from 28 dB to 47 dB, i.e. errors are very large. As it follows from [45], $HaarPSI_{des}$ cannot be provided by the BPG coder with appropriate accuracy using fixed *Q* as well. Certainly, we have not checked all coders and all metrics but it seems that it is difficult to reach our goal using fixed PCC.

Then, some trade-off is needed. This can be a two-step approach described in detail in the thesis of L. Fangfang [60] and the basic papers [15, 16, 61–64]. The idea is the following. Let's obtain RDCs of interest in advance for a set of test images with various properties and get the average RDC for them with estimation of derivative values for different fragments of this curve. Then, for a given image to be compressed by a given coder with providing a given $Metr_{des}$, let's determine PCC_1 (a starting PCC) that corresponds to $Metr_{des}$ for the average curve. Then, carry out compression and decompression for the considered image using PCC_1 and estimate $Metr_1$ for the decompressed image. If $Metr_1$ does not differ from $Metr_{des}$ essentially (i.e. $|Metr_1 - Metr_{des}| < \delta_M$ where δ_M is the allowed error), then stop and keep the compressed image as the desired result. If no, calculate PCC_2 as

$$PCC_2 = PCC_1 + \left(Metr_{des} - Metr_1\right) \Big/ \left(dMetr\left(PCC_1\right) / dPCC\right), \tag{1.2}$$

where rounding-off should be applied if *PCC* can be only integer.

As seen, linear approximation of the RDCs based on the average curve is applied within this approach. This explains both its advantages and shortcomings. The advantages are twofold. First, the method usually provides about one order less errors (variance) of providing $Metr_{des}$ after the second step than after the first step where improvement is provided almost for all images and in the wide range of $Metr_{des}$ [16, 60, 63]. Second, the procedure of compression with providing a given $Metr_{des}$ usually takes considerably less time than iterative procedures described above since only two compressions and one decompression are needed (and sometimes the second compression is not needed at all). The two-step procedure occurs to be efficient for RDCs presented in **Fig. 1.8, *b***.

The main shortcomings are considered in [65]. First, it might be so that the mean of $Metr_2$ is biased and then one has to take into account not only variance of the provided metric values but the bias as well. This happens if the absolute value of the second derivative of the average curve in PCC_1 is large enough. Till the moment, no attempts to take into account the second derivative have been undertaken. Second, due to the nonlinearity of the average curve, it might be so that the determined PCC_2 occurs to be negative. This is in contradiction with assumptions concerning the range of PCC (for all types of PCC, it can be only positive).

Let's consider such "bad" situations. Suppose that one has to provide $PSNR_{des} = 30$ dB for the AGU coder. Then, QS_1 is set equal to 60.15. There are test images (Goldhill, Barbara) for which $PSNR_{des}$ is provided with appropriate accuracy, i.e. with the errors less than 1 dB) even for QS_1 although the second step provides practically perfect result. Meanwhile, there are images (e.g., Baboon, Frisco, and Diego) for which $PSNR_1$ differs from $PSNR_{des}$ significantly. After the second step, the situation does not radically improve since the errors are still about 3–5 dB for such textural images as Diego and Baboon. The reason for this is large difference QS_1QS_2, i.e. QS_1 and QS_2 differ a lot and linear approximation of the particular and average RDCs is not valid anymore. Finally, there are images (Lenna, Aerial) for which the second step improves accuracy (decreases the errors) of $PSNR_{des}$ providing. Due to such images as Diego and Baboon, variance after the second step does not decrease significantly compared to variance after the first step (**Table 1.2**).

Table 1.2 Statistics and parameters of providing $PSNR_{des} = 30$ dB for a set of test images

Test image	QS_1	$PSNR_1$	ΔQS	QS_2	$PSNR_{prov}$
Goldhill	60.15	30.34	4.24	64.39	29.98
Baboon	60.15	26.72	–40.2	19.87	33.97
Barbara	60.15	30.88	10.87	71.01	29.95
Lenna	60.15	32.62	32.35	92.50	30.72
Aerial	60,15	28.34	–20.4	39.68	30.69
Airfield	60.15	27.05	–36.3	23.80	32.52
Frisco	60.15	34.68	57.62	117.7	31.16
Diego	60.15	26.44	–43.83	16.31	35.21
$Mrt_{\_prepared}$	60.15	32.89	35.66	95.81	24.51
Variance		9.12			9.05

Then, special restrictions can be imposed [66]. For example, PCC_2 is set equal to $PCC_1/2$ if the calculated PCC_2 is less than $PCC_1/2$. This does not allow PCC_2 to be negative (since PCC_1 is always positive) and, in fact, restricts the area where linear

approximation is considered appropriate. Third, there are cases (RDCs for particular images) where dependences *Metr*(*PCC*) and *dMetr*(*PCC*$_1$)/*dPCC* for a given image to be compressed differs from the average curve and derivative a lot (see **Fig. 1.8, *c, d***). Then, although the two-step procedure improves the accuracy considerably, this accuracy is still inappropriate [67]. A way out is proposed in [61] where it is taken into account that the DCT-based coder AGU provides almost the same compression characteristics as SPIHT and CR for the AGU coder can be easily predicted. One more solution to improve accuracy of providing $Metr_{des}$ has been proposed in [62, 64]. It has been taken into account that RDCs usually depend on image complexity. Then, it is possible to obtain average curves for simple and complex structure images in advance. For a given image to be compressed, its complexity is determined first, and after this, based on such a pre-classification, the corresponding average RDC is used within the two-step procedure to determine PCC_2.

Although the trade-off had been found, the desire was still to design an approach to adaptive compression without decompression and the second step of compression. Because of this, in parallel with the design of the two-step approach, the approaches based on prediction have been studied [10, 68–70]. The idea put behind the approach proposed in [68] is that, for JPEG with uniform quantization, MSE of distortions introduced due to quantizing DCT coefficients in blocks is equal to MSE of distortions observed in the corresponding decompressed image blocks, i.e., in spatial domain. Then, it is possible to calculate aggregate MSE_{DCT} in the DCT domain for a given *QS* and estimate (predict) MSE_{spat} of distortions after decompression (due to compression). MSE in DCT domain with averaging the local estimates for all blocks can be expressed as

$$MSE_{DCT} = \frac{1}{63N}\sum_{n=1}^{N}\left(\sum_{i=1}^{63}\left(QS \times round\left(\frac{D_i}{QS}\right) - D_i\right)^2\right), \tag{1.3}$$

where D_i is the value of the i-th DCT coefficient in a processed n-th block, N denotes the number of analyzed blocks, 63 AC (alternating current) DCT coefficients are analyzed, round denotes rounding-off to the nearest integer. The value MSE_{spat} has been shown to be approximately equal to MSE_{DCT}. In addition, it has been demonstrated that there is no need to take all possible 8 × 8 pixel blocks to calculate MSE_{DCT}. It was enough to have 500 blocks. Since DCT in 8 × 8 pixel blocks is a fast operation, prediction for a given *QS* is very fast. Moreover, it has been shown [68], that, using correcting factors with values close to unity, it is possible to predict MSE for given *QS* for the AGU and ADCT coders. The prediction accuracy was shown to be better than for the procedure in [71].

The paper [69] shows that the same prediction can be carried out for non-uniform quantization often used in JPEG and employed in the AGU-M and ADCT-M coders. For the latter two coders that, in fact, use 32 × 32 pixel and adaptive block size, respectively, the prediction based on 8 × 8 pixel blocks is shown possible with correction factors of about 0.9 and relative error less than 10 %, i.e. smaller than 0.4 dB which is appropriate for practice. The prediction approach is tested in [69] for a wide set of images of different origin.

The paper [70] proposes another approach to prediction. It is shown [10, 12, 70] that for small *QS* for DCT-based coders the *MSE* of introduced distortions is often proportional to QS^2 and approximately equal to $QS^2/12$. For larger *QS*, the dependence becomes less fast than ~QS^2 and depends on image complexity. Then, it is proposed to predict *MSE* as

$$MSE \approx \left(QS^2/12\right) f(X), \tag{1.4}$$

where $f(X)$ is some function of one or several parameters describing image complexity. As one option, the use of probability P_0 that DCT coefficients in 8 × 8 pixel blocks occur to be zero after quantization using a given *QS* is considered. This probability is small for small *QS* and it increases if *QS* becomes larger. Note that for $P_0 < 0.6$ the function $f(X)$ slowly decreases but it is almost equal to unity. Decreasing speed increases if P_0 exceeds 0.6. The approximations are given in [70] and for $P_0 \approx 0.9$ one has $f(X) \approx 0.6$, but the accuracy is not good enough.

Let's note that the approach [70] is based on obtaining the scatter-plot for a set of test images compressed with different *QS*. Slightly other approaches are studied in [12, 72]. In [72], it is shown that there is an essential dependence between image entropy *E* (that deals with image complexity of noise-free images) and MSE of introduced distortions for the BPG coder applied to grayscale images. One example from the paper [72] is presented in **Fig. 1.12** where MSE values are given for 21 test images compressed with $Q = 25$. The obtained results show the following: can vary from about 4 to 8 where for most images *E* exceeds 7.0 and the MSE values about 6 are observed for them. Meanwhile, there are also quite many images having smaller entropy and MSE values for them are considerably smaller (except the test image Goldhill). This example, as well as other examples given in [72], show that there is a considerable correlation between MSE and *E*. Further studies [74] have shown that MSE has a certain degree of correlation with other parameters characterizing complexity and the joint use of such parameters can improve prediction where PCC and a few parameters characterizing complexity are jointly used as inputs of a very simple trained neural network.

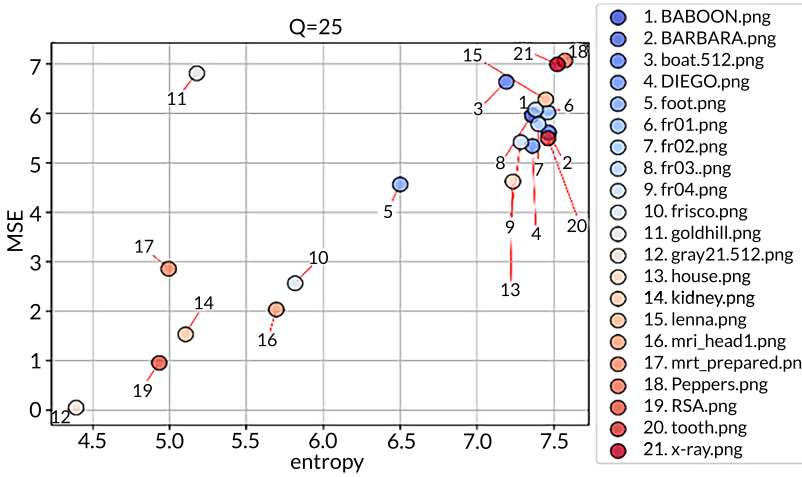

Fig. 1.12 Scatter-plot of MSE vs *E* for grayscale images compressed by the BPG coder

The data in [72, 73] partially explain why MSE of introduced distortions is usually larger for more complex structure images. A detailed local analysis of distortion statistics is carried out and it is shown that distortions are larger in image regions (blocks) having higher activity characterized by local variance. Then, if an image has more blocks identified as locally active, integral MSE should be larger. To illustrate this phenomenon, **Fig. 1.13** presents two maps for the test image Frisco (**Table 1.1**, the rightmost image): the map of local activity (**Fig. 1.13, *a***, more active blocks are shown by lighter color) and the map of local MSEs of distortions (**Fig. 1.13, *b***, larger MSEs are indicated by brighter color). As seen, there is a high "correlation" between these two maps.

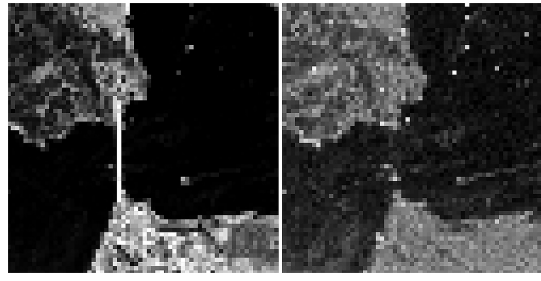

a *b*

Fig. 1.13 The local activity map (*a*) and the map of local MSEs of distortions due to lossy compression (*b*)

Currently, the accuracy of MSE prediction by the methods described above is at the same order as for the two-step methods. The task dealing with MSE prediction is that the prediction does not directly solve the problem of providing MSE_{des}. Then, one has to start from some PCC_{start} and predict MSE_{start} for it. If this MSE_{start} differs from MSE_{des} considerably (more than allowed), PCC has to be changed accordingly (one way to do this is described in [72]). Then, the processing becomes two-step but, recall, there is no need to compress and decompress the image at the first step. Thus, the compression with providing MSE_{des} can be faster than for two-step method described above if prediction requires less time expenses than compression and decompression. This is (could be) the main advantage of the approaches based on prediction. However, there are also several drawbacks. First, currently, the prediction approach has been mainly oriented on determining MSE or, equivalently, PSNR. Then, it is needed to check whether or not this approach allows predicting visual quality metrics. Second, the trade-off between complexity and accuracy of prediction has to be found for coders under interest. Third, fast and accurate algorithms of setting PCC for final compression have to be designed and tested.

Finally, let's consider the case of visually lossless compression based on JND No. 1 [9, 75]. This approach presumes that, depending on an image property indicator, a metric or PCC value ($Metr_{JND}$ or PCC_{JND}) that corresponds to JND No. 1 is determined and, then, this value is provided. The approach is based on preliminary analysis for special databases (such as KonJND-1k [76] and some others) that contain many images for which JND No. 1 points have been estimated for a considered coder by experiment participants.

Some results of experiments for JPEG are demonstrated in **Fig. 1.14** taken from [9]. JND No. 1 point for each RDC is illustrated by ×. The following conclusions can be drawn:

1) JND No. 1 points are observed for a wide range of QF and PSNR values (**Fig. 1.14, *a***), for a narrower range of PSNR-HVS-M values (**Fig. 1.14, *b***), and a wide range of bpp values (**Fig. 1.14, *c***); there are some (rarely met) images for which even the use of QF ≈ 80 does not guarantee invisibility of distortions whilst for some images the distortions are invisible for QF ≈ 30;

2) there are some curves PSNR(QF) and PSNR-HVS-M(QF) that are not monotonous corresponding to the so-called strange images [14] for which many methods of providing $Metr_{des}$ might have problems.

Let's give a few examples of strange images and RDCs for them. **Fig. 1.15** presents natural scene color image (**Fig. 1.15, *a***) and RDC PSNR vs QF for JPEG (**Fig. 1.15, *b***). As seen, the image has a large quasi-homogeneous dark region and the curve has jumps with the amplitude reaching 1 dB. An example of remote sensing image is giv-

en in **Fig. 1.16, *a*** and RDCs PSNR vs QS for color and intensity components compressed by the AGU coder are presented in **Fig. 1.16, *b***. Obviously, all four curves have "fluctuations" and are not monotonous.

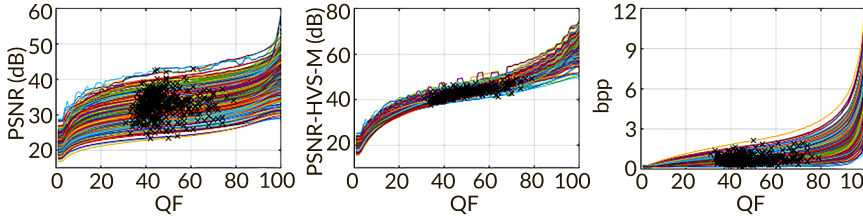

a *b* *c*

Fig. 1.14 RDCs PSNR (*a*), PSNR-HVS-M (*b*), and bpp (*c*) on QF, along with JND No. 1 points, for a subset of scene color images taken from the KonJND-1k database and compressed by JPEG

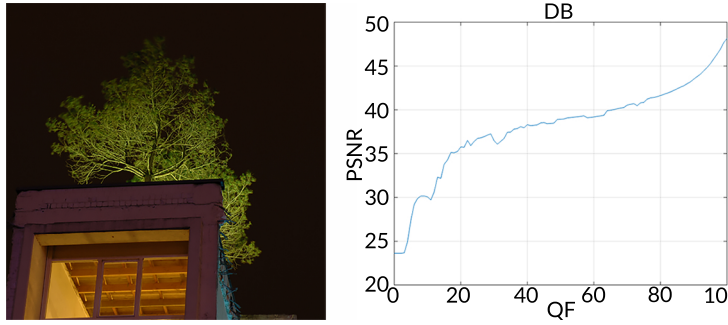

a *b*

Fig. 1.15 Natural scene color image (*a*) and RDC PSNR vs QF for JPEG (*b*)

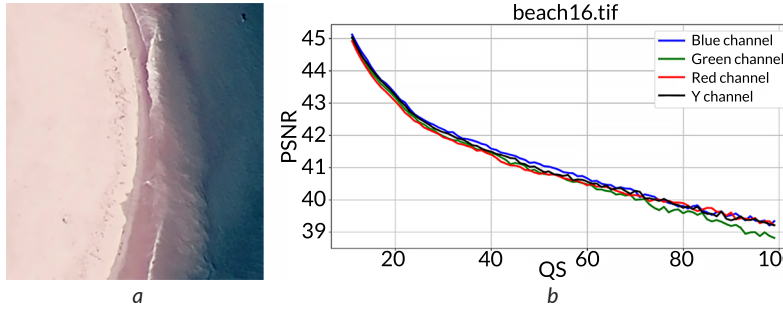

a *b*

Fig. 1.16 Remote sensing image (*a*) and the RDCs PSNR vs QS for AGU (*b*)

Fig. 1.17 shows two other color images that occur to be strange if the dependence PSNR(QF) for JPEG is considered. Joint analysis of images in **Fig. 1.15, *a***, **Fig. 1.16, *a***, and **Fig. 1.17** shows that images can be strange if they contain large dark, or white (e.g., overexposed images) or other color regions. This assumption has been checked for artificial color image presented in **Fig. 1.18, *a*** compressed by JPEG and the assumption has been confirmed (see RDC of *PSNR* vs *QF* in **Fig. 1.18, *b***).

a *b*

Fig. 1.17 Examples of two strange images: example 1 (*a*) and example 2 (*b*)

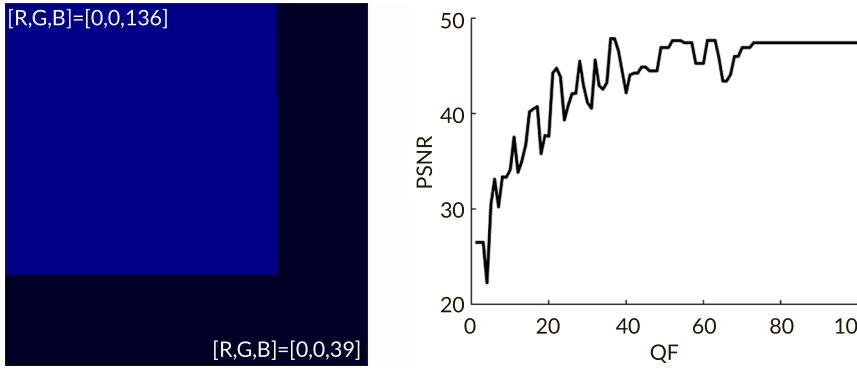

a *b*

Fig. 1.18 Artificial color test image with large homogeneous regions (*a*) and RDC PSNR vs QF for JPEG (*b*)

It might seem that strange images take place only according to PSNR and mainly for JPEG. However, this is not true. **Fig. 1.19** shows dependencies of PSNR and MDSI metrics on QF for intensity component of the color image beach16 represented in **Fig. 1.16, *a***. As seen, beach16 is the strange image not only according to PSNR but also according to the visual quality metric MDSI. Note that the largest "fluctuations" of MDSI take place in the same interval of QF as for PSNR – for QF about 10.

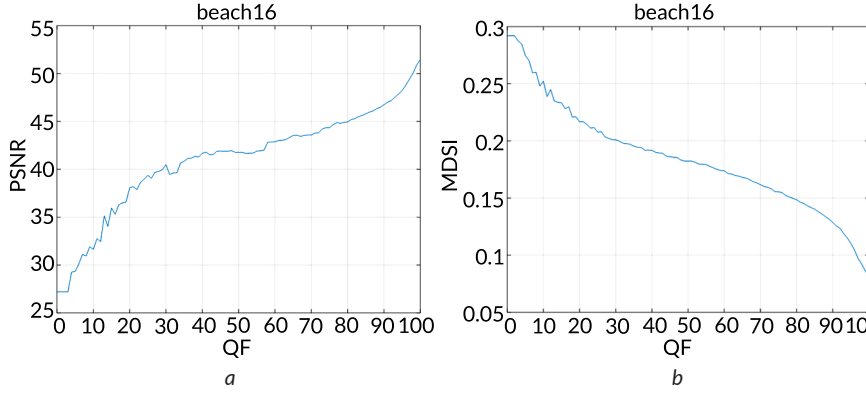

a *b*

Fig. 1.19 Dependencies PSNR (*a*) and MDSI metric (*b*) on QF for intensity component of the color image beach16

The images strange for JPEG often occur to be strange for the coder AGU. This is not surprising since both use DCT in blocks as the basis for lossy compression.

In addition, not only color images can be strange – grayscale images can be strange as well especially those ones having large homogeneous backgrounds, e.g., images of text documents or advertising materials.

The cases and reasons for strange images are discussed in [14, 77]. Currently, we deal with detection of strange images before compression.

Let's come back to considering JND No. 1. It is shown in [9] that there are many image property (complexity) indicators that are correlated with parameters of JND No. 1. Mean spatial frequency SF_{mean} that can be quite easily calculated has the largest correlation [75]. This can be seen by analysis of scatter-plots in **Fig. 1.20**. Such scatter-plots have allowed to provide the following rules for determining PSNR for JPEG and BPG, respectively:

$$PSNR(SF_{mean}) = \begin{cases} 0.01376SF_{mean}^2 - 0.8645SF_{mean} + 38.97, & SF_{mean} \le 31; \\ 25.4, & SF_{mean} > 31. \end{cases} \quad (1.5)$$

$$PSNR\left(SF_{mean}\right)=\begin{cases}0.01336SF_{mean}^{2}-0.7618SF_{mean}+40.36, & SF_{mean}\le 28;\\ 29.5, & SF_{mean}>28.\end{cases} \quad (1.6)$$

More details can be found in [14, 75, 78, 79]. Thus, either the metric value or PCC that correspond to JND No. 1 can be determined and the next step is to provide it. As shown above, this task can be solved by the two-step or prediction approaches.

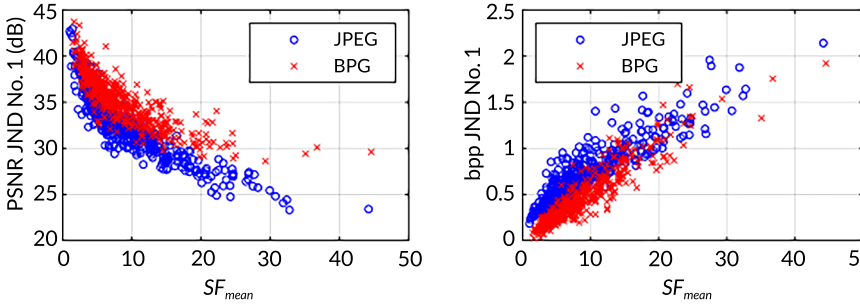

a *b*

Fig. 1.20 Scatter-plots of PSNR (*a*) and *bpp* (*b*) vs SF_{mean} for the first JND points determined using KonJND-1k image subsets for JPEG and BPG coders

The JND No. 1 position represents the boundary between visually lossless and visually lossy compression. Therefore, these positions can be used in the assessment and analysis of image quality [80]. Thus, **Fig. 1.21** illustrates how PSNRs that correspond to JND No. 1 can be used to detect high quality images ($PSNR > PSNR_{JND\ No.\ 1}$). In the quality analysis, well-known publicly available image datasets from the visible (LIVE and VCL@FER) and the infrared part of the electromagnetic spectrum (long wave infrared – LWIR [80]) are used. Using $PSNR_{JND\ No.\ 1}$, JPEG compressed images of excellent quality are detected in LIVE (see lower difference MOS (DMOS) values, **Fig. 1.21, *a***) and LWIR datasets (higher MOS values, **Fig. 1.21, *c***), while for the VCL@FER database there are several exceptions with good quality images (**Fig. 1.21, *b***).

The results in [79] demonstrate that the influence of compression at the JND No. 1 does not significantly affect the target detection by humans. This allows compressing images in adaptive way instead of using fixed QF for JPEG with saving memory effectively. Meanwhile, accuracy of approaches based on JND No. 1 needs additional study.

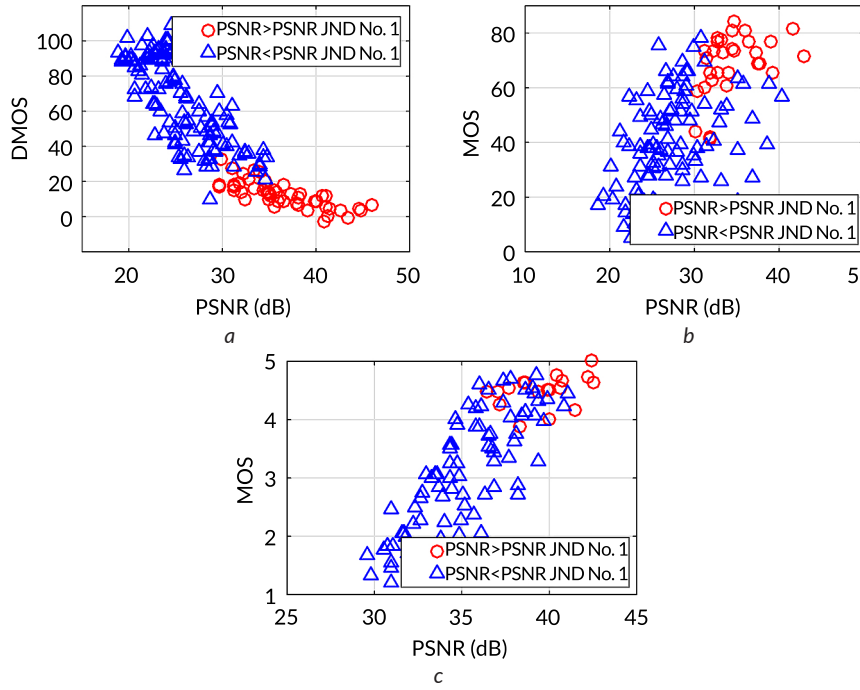

Fig. 1.21 Scatter plots of PSNR and subjective quality scores for JPEG images from three datasets (*a*) LIVE (175 images), (*b*) VCL@FER (138 images) and (*c*) LWIR (100 images)

We would like to discuss some limitations of the considered approaches. First, if one wants to apply the two-step approach for a new metric and/or a new coder, the corresponding average RDC and its derivative have to be obtained. This is not a difficult work and it has to be done once. Some other drawbacks and limitations of the two-step approach are considered in [65].

Second, the method of MSE and MSE_{HVSM} prediction [68–70, 72] has been tested for several DCT-based compression techniques. However, it is not clear can it be adapted to wavelet-based coders. Besides, it is not clear can the approach be applied to prediction of other metrics. The approach to MSE prediction based on indicators of image complexity [12] is at the beginning of its design and it has been tested only for the BPG encoder. It is possible to expect that the approach should be useful for other compression techniques, but to be general, it has to be modified and verified for other coders.

Finally, the approach based on JND [9, 80] presumes the use of several databases of distorted images and the results of their quality assessment by a great number of experiment participants. Such experiments are labor and time consuming and have to be carried out for each compression technique under interest. However, such experiments can be done once and then the obtained results can be used for several purposes.

1.7 Conclusions and future research directions

Summarizing the presented materials, it is possible to conclude the following:

1. There are quite many metrics of visual quality that are able to quite adequately perform for lossy compression of images.

2. In general, there are several ways to provide a desired quality according to the chosen metric; advantages and drawbacks of these ways have been discussed above from the viewpoints of accuracy and time needed for their realization.

3. Some of these ways can be further advanced; this relates to the two-step methods, algorithms based on prediction, and methods relating to JND No. 1.

4. More research should be done for prediction of visual quality metrics, especially for color and multichannel images.

5. Strange images have to be considered more in detail; reliable and fast detection of potential strange images before lossy compression is a task to be solved.

6. Approaches to image quality providing for modern coders such as HEIF and AVIF has to be studied; to the best of our knowledge, the corresponding research has not been carried out yet.

7. Applicability of the considered approaches to providing the quality of infrared images has to be studied as well.

8. It is also worth continuing studies of lossy compression impact on classification and recognition of images and remote sensing data.

Conflict of interest

The authors declare that there is no conflict of interest in relation to this paper, as well as the published research results, including the financial aspects of conducting the research, obtaining and using its results, as well as any non-financial personal relationships.

Financing

The study was performed without financial support.

Data availability

Data will be made available on reasonable request.

Use of artificial intelligence statement

The authors confirm that they did not use artificial intelligence technologies when creating the current work.

Authors' contributions

Volodymyr Lukin: Conceptualization, Supervision, Writing – review & editing.
Sergii Kryvenko: Data curation, Investigation.
Fangfang Li: Methodology, Writing – original draft, Software.
Sergiy Abramov: Methodology, Data curation.
Viktoriia Abramova: Project administration, Data curation.
Bohdan Kovalenko: Resources, Software.
Igor Dohtiev: Software, Formal analysis.
Oleksandr Arkhipov: Software, Formal analysis.
Nenad Stojanović: Formal analysis, Writing – original draft, Software.
Boban Bondžulić: Methodology, Data curation, Resources.

References

1. Wei, J., Mi, L., Hu, Y., Ling, J., Li, Y., Chen, Z. (2022). Effects of Lossy Compression on Remote Sensing Image Classification Based on Convolutional Sparse Coding. IEEE Geoscience and Remote Sensing Letters, 19, 1–5. https://doi.org/10.1109/lgrs.2020.3047789
2. Dougherty, G. (2009). Digital Image Processing for Medical Applications. Cambridge: Cambridge University Press. https://doi.org/10.1017/cbo9780511609657

3. Doss, S., Pal, S., Akila, D., Jeyalaksshmi, S., Jabeen, T. N., Suseendran, G. (2020). Satellite image remote sensing for identifying aircraft using SPIHT and NSCT. Journal of Critical Reviews, 7 (5), 631–634. https://doi.org/10.31838/jcr.07.05.130
4. Zabala, A., Pons, X. (2011). Effects of lossy compression on remote sensing image classification of forest areas. International Journal of Applied Earth Observation and Geoinformation, 13 (1), 43–51. https://doi.org/10.1016/j.jag.2010.06.005
5. Radosavljević, M., Brkljač, B., Lugonja, P., Crnojević, V., Trpovski, Ž., Xiong, Z., Vukobratović, D. (2020). Lossy Compression of Multispectral Satellite Images with Application to Crop Thematic Mapping: A HEVC Comparative Study. Remote Sensing, 12 (10), 1590. https://doi.org/10.3390/rs12101590
6. Lyalko, V., Popov, M., Sedlerova, O., Fedorovskyi, O., Stankevich, S., Yelistratova, L. et al. (2022). On the development of remote sensing methods and technologies in Ukraine. Ukrainian Journal of Remote Sensing, 9 (2), 43–53. https://doi.org/10.36023/ujrs.2022.9.2.214
7. Altamimi, A., Ben Youssef, B. (2024). Lossless and Near-Lossless Compression Algorithms for Remotely Sensed Hyperspectral Images. Entropy, 26 (4), 316. https://doi.org/10.3390/e26040316
8. Christophe, E.; Prasad, S., Bruce, L. M., Chanussot, J. (Eds.) (2011). Hyperspectral Data Compression Tradeoff. Optical Remote Sensing. Berlin, Heidelberg: Springer 9–29. https://doi.org/10.1007/978-3-642-14212-3_2
9. Bondžulić, B., Stojanović, N., Lukin, V., Kryvenko, S. (2024). JPEG and BPG visually lossless image compression via KonJND-1k database. Vojnotehnicki Glasnik, 72 (3), 1214–1241. https://doi.org/10.5937/vojtehg72-50300
10. Krivenko, S. S., Krylova, O., Bataeva, E., Lukin, V. V. (2018). Smart lossy compression of images based on distortion prediction. Telecommunications and Radio Engineering, 77 (17), 1535–1554. https://doi.org/10.1615/telecomradeng.v77.i17.40
11. Kovalenko, B., Lukin, V. (2023). Analysis of distortions due to BPG-based lossy compression of noise-free and noisy images. Herald of Khmelnytskyi National University. Technical sciences, 325 (5), 128–135.
12. Kovalenko, B., Lukin, V. (2024). Pre-Requisites for Mean Square Error Prediction in Better Portable Graphics Based Lossy Compression of Grayscale Images. 2024 IEEE 42nd International Conference on Electronics and Nanotechnology (ELNANO). Kyiv, 488–492. https://doi.org/10.1109/elnano63394.2024.10756949
13. Zemliachenko, A., Lukin, V., Ponomarenko, N., Egiazarian, K., Astola, J. (2015). Still image/video frame lossy compression providing a desired visual quality. Multidimensional Systems and Signal Processing, 27 (3), 697–718. https://doi.org/10.1007/s11045-015-0333-8

14. Bondzulic, B., Bujakovic, D., Li, F., Lukin, V. (2022). On strange images with application to lossy image compression. Radioelectronic and Computer Systems, 4, 143–152. https://doi.org/10.32620/reks.2022.4.11
15. Li, F., Lukin, V., Okarma, K., Fu, Y. (2021). Providing a Desired Quality of BPG Compressed Images for FSIM Metric. 2021 IEEE 3rd International Conference on Advanced Trends in Information Theory (ATIT). Kyiv, 10–14. https://doi.org/10.1109/atit54053.2021.9678522
16. Li, F., Lukin, V., Ieremeiev, O., Okarma, K. (2022). Quality Control for the BPG Lossy Compression of Three-Channel Remote Sensing Images. Remote Sensing, 14 (8), 1824. https://doi.org/10.3390/rs14081824
17. Bondžulić, B., Pavlović, B., Stojanović, N., Petrović, V., Bujaković, D. (2023). A simple and reliable approach to providing a visually lossless image compression. The Visual Computer, 40 (5), 3747–3763. https://doi.org/10.1007/s00371-023-03062-y
18. Ponomarenko, N. N., Lukin, V. V., Egiazarian, K. O., Lepisto, L. (2013). Adaptive visually lossless JPEG-based color image compression. Signal, Image and Video Processing, 7 (3), 437–452. https://doi.org/10.1007/s11760-013-0446-1
19. Makarichev, V., Vasilyeva, I., Lukin, V., Vozel, B., Shelestov, A., Kussul, N. (2021). Discrete Atomic Transform-Based Lossy Compression of Three-Channel Remote Sensing Images with Quality Control. Remote Sensing, 14 (1), 125. https://doi.org/10.3390/rs14010125
20. Makarichev, V., Lukin, V., Brysina, I. (2024). On the Impact of Discrete Atomic Compression on Image Classification by Convolutional Neural Networks. Computation, 12 (9), 176. https://doi.org/10.3390/computation12090176
21. Jia, S., Ji, Z., Qian, Y., Shen, L. (2012). Unsupervised Band Selection for Hyperspectral Imagery Classification Without Manual Band Removal. IEEE Journal of Selected Topics in Applied Earth Observations and Remote Sensing, 5 (2), 531–543. https://doi.org/10.1109/jstars.2012.2187434
22. Ponomarenko, N. N., Lukin, V. V., Zriakhov, M. S., Kaarna, A., Astola, J. (2008). Automatic Approaches to On-Land/On-Board Filtering and Lossy Compression of AVIRIS Images. IGARSS 2008 – 2008 IEEE International Geoscience and Remote Sensing Symposium. Boston, III-254–III–257. https://doi.org/10.1109/igarss.2008.4779331
23. Lukin, V., Krivenko, S., Li, F., Abramov, S., Makarichev, V. (2022). On Image Complexity in Viewpoint of Image Processing Performance. Information technologies and systems of information security. IntelITSIS-2022, 16.
24. Bondžulić, B., Lukin, V., Bujaković, D., Li, F., Kryvenko, S., Pavlović, B. (2023). On Visually Lossless JPEG Image Compression. 2023 Zooming Innovation in

Consumer Technologies Conference (ZINC), 113–118. https://doi.org/10.1109/zinc58345.2023.10174090
25. Zhang, Y., Zhang, Z., Wang, X., Wang, X., Ge, J., Bian, F. (2018). An Adaptive Infrared Image Preprocessing Method Based on Background Complexity Descriptors. 2018 Eighth International Conference on Instrumentation & Measurement, Computer, Communication and Control (IMCCC), 344–349. https://doi.org/10.1109/imccc.2018.00079
26. Abramova, V. V. (2015). A blind method for additive noise variance evaluation based on homogeneous region detection using the fourth central moment analysis. Telecommunications and Radio Engineering, 74 (18), 1651–1669. https://doi.org/10.1615/telecomradeng.v74.i18.50
27. Lukin, V., Kryvenko, S., Bondzulic, B., Bujakovic, N. (2024). Compression Ratio Behavior for BPG-based Compression of Grayscale Images. Proceedings of ATIT. Lviv. (in print).
28. Lukac, R., Plataniotis, K. N. (Eds.) (2007). Color Image Processing: Methods and Applications. Image processing series. Boca Raton: CRC/Taylor & Francis.
29. Jayachandran, S. (2017). Digital imaging in dentistry: A review. Contemporary Clinical Dentistry, 8 (2), 193–194. https://doi.org/10.4103/ccd.ccd_535_17
30. Krivenko, S., Lukin, V., Krylova, O., Kryvenko, L., Egiazarian, K. (2020). A Fast Method of Visually Lossless Compression of Dental Images. Applied Sciences, 11 (1), 135. https://doi.org/10.3390/app11010135
31. Flint, A. C. (2012). Determining optimal medical image compression: psychometric and image distortion analysis. BMC Medical Imaging, 12 (1). https://doi.org/10.1186/1471-2342-12-24
32. Lin, W., Jay Kuo, C.-C. (2011). Perceptual visual quality metrics: A survey. Journal of Visual Communication and Image Representation, 22 (4), 297–312. https://doi.org/10.1016/j.jvcir.2011.01.005
33. Chandler, D. M. (2013). Seven Challenges in Image Quality Assessment: Past, Present, and Future Research. ISRN Signal Processing, 2013, 1–53. https://doi.org/10.1155/2013/905685
34. Moorthy, A. K., Bovik, A. C. (2010). Visual quality assessment algorithms: what does the future hold? Multimedia Tools and Applications, 5 1(2), 675–696. https://doi.org/10.1007/s11042-010-0640-x
35. Andrew, B. W. (1993). DCTune: A technique for visual optimization of DCT quantization matrices for individual images. Society for Information Display Digest of Technical Papers, 946–949.
36. Bosse, S., Maniry, D., Muller, K.-R., Wiegand, T., Samek, W. (2018). Deep Neural Networks for No-Reference and Full-Reference Image Quality Assessment.

IEEE Transactions on Image Processing, 27 (1), 206–219. https://doi.org/10.1109/tip.2017.2760518
37. Lukin, V., Abramov, S., Krivenko, S., Kurekin, A., Pogrebnyak, O. (2013). Analysis of classification accuracy for pre-filtered multichannel remote sensing data. Expert Systems with Applications, 40 (16), 6400–6411. https://doi.org/10.1016/j.eswa.2013.05.061
38. Ponomarenko, N., Silvestri, F., Egiazarian, K., Carli, M., Astola, J., Lukin, V. (2007). On between-coefficient contrast masking of DCT basis functions. CD-ROM Proceedings of VPQM, 4.
39. Lukin, V., Ponomarenko, N., Egiazarian, K., Astola, J. (2015). Analysis of HVS-Metrics' Properties Using Color Image Database TID2013. Proceedings of ACIVS. Italy, 613–624. https://doi.org/10.1007/978-3-319-25903-1_53
40. Ieremeiev, O. I., Lukin, V. V., Ponomarenko, N. N., Egiazarian, K. O., Astola, J. (2016). Combined full-reference image visual quality metrics. Electronic Imaging, 28 (15), 1–10. https://doi.org/10.2352/issn.2470-1173.2016.15.ipas-180
41. Ponomarenko, N., Ieremeiev, O., Lukin, V., Egiazarian, K., Jin, L., Astola J. (2013). Color Image Database TID2013: Peculiarities and Preliminary Results, Proceedings of EUVIP. Paris, 106–111.
42. Varga, D. (2020). A Combined Full-Reference Image Quality Assessment Method Based on Convolutional Activation Maps. Algorithms, 13 (12), 313. https://doi.org/10.3390/a13120313
43. Ieremeiev, O., Lukin, V., Okarma, K., Egiazarian, K. (2020). Full-Reference Quality Metric Based on Neural Network to Assess the Visual Quality of Remote Sensing Images. Remote Sensing, 12 (15), 2349. https://doi.org/10.3390/rs12152349
44. Okarma, K.; Rutkowski, L., Scherer, R., Tadeusiewicz, R., Zadeh, L. A., Zurada, J. M. (Eds.) (2010). Combined Full-Reference Image Quality Metric Linearly Correlated with Subjective Assessment. Artificial Intelligence and Soft Computing. Berlin, Heidelberg: Springer, 539–546. https://doi.org/10.1007/978-3-642-13208-7_67
45. Li, F., Ieremeiev, O., Lukin, V., Egiazarian, K. (2024). BPG-Based Lossy Compression of Three-Channel Remote Sensing Images with Visual Quality Control. Remote Sensing, 16 (15), 2740. https://doi.org/10.3390/rs16152740
46. Ziaei Nafchi, H., Shahkolaei, A., Hedjam, R., Cheriet, M. (2016). Mean Deviation Similarity Index: Efficient and Reliable Full-Reference Image Quality Evaluator. IEEE Access, 4, 5579–5590. https://doi.org/10.1109/access.2016.2604042
47. Reisenhofer, R., Bosse, S., Kutyniok, G., Wiegand, T. (2018). A Haar wavelet-based perceptual similarity index for image quality assessment. Signal Processing: Image Communication, 61, 33–43. https://doi.org/10.1016/j.image.2017.11.001

48. Zhang, L., Zhang, L., Mou, X., Zhang, D. (2011). FSIM: A Feature Similarity Index for Image Quality Assessment. IEEE Transactions on Image Processing, 20 (8), 2378–2386. https://doi.org/10.1109/tip.2011.2109730
49. Ieremeiev, O., Lukin, V., Okarma, K., Egiazarian, K., Vozel, B. (2022). On properties of visual quality metrics in remote sensing applications. Electronic Imaging, 34 (10), 354-1-354–356. https://doi.org/10.2352/ei.2022.34.10.ipas-354
50. Barman, N., Martini, M. G. (2020). An Evaluation of the Next-Generation Image Coding Standard AVIF. 2020 Twelfth International Conference on Quality of Multimedia Experience (QoMEX). Athlone: IEEE. https://doi.org/10.1109/qomex48832.2020.9123131
51. Lainema, J., Hannuksela, M. M., Vadakital, V. K. M., Aksu, E. B. (2016). HEVC still image coding and high efficiency image file format. 2016 IEEE International Conference on Image Processing (ICIP), 71–75. https://doi.org/10.1109/icip.2016.7532321
52. Taubman, D. S., Marcellin, M. W. (2002). JPEG2000 Image Compression Fundamentals, Standards and Practice. Springer US. https://doi.org/10.1007/978-1-4615-0799-4
53. Beong-Jo Kim, Pearlman, W. A. (1997). An embedded wavelet video coder using three-dimensional set partitioning in hierarchical trees (SPIHT). Proceedings DCC'97. Data Compression Conference. Snowbird: IEEE Comput. Soc. Press, 251–260. https://doi.org/10.1109/dcc.1997.582048
54. Ponomarenko, N., Lukin, V., Egiazarian, K., Astola, J. (2005). DCT Based High Quality Image Compression. Image Analysis. Joensuu, 1177–1185. https://doi.org/10.1007/11499145_119
55. Ponomarenko, N. N., Egiazarian, K. O., Lukin, V. V., Astola, J. T. (2007). High-Quality DCT-Based Image Compression Using Partition Schemes. IEEE Signal Processing Letters, 14 (2), 105–108. https://doi.org/10.1109/lsp.2006.879861
56. Lukin, V., Abramov, S., Kozhemiakin, R., Rubel, A., Uss, M., Ponomarenko, N. et al.; Emre Celebi, M., Lecca, M., Smolka, B. (2015). DCT-Based Color Image Denoising: Efficiency Analysis and Prediction. Color Image and Video Enhancement. Springer, 55–80. https://doi.org/10.1007/978-3-319-09363-5_3
57. Zriakhov, M. S., Lukin, V. V. (2005). Obespechenie zadannogo kachestva pri szhatii izobrazhenii s poteriami. Radiotekhnika, 143, 76–82.
58. Zemliachenko, A. N., Kolganova, O. E., Lukin, V. V. (2011). Acceleration image compression with required visual quality. Radioelektronnye i kompiuternye sistemy, 4 (52), 52–59.

59. Kryvenko, L., Krylova, O., Lukin, V., Kryvenko, S. (2024). Intelligent visually lossless compression of dental images. Advanced Optical Technologies, 13. https://doi.org/10.3389/aot.2024.1306142
60. Li, F. (2023). Design and analysis of efficient methods for providing a desired quality in image lossy compression. [Extended abstract of PhD thesis; National Aerospace University].
61. Li, F., Krivenko, S., Lukin, V.; Nechyporuk, M., Pavlikov, V., Kritskiy, D. (Eds.) (2021). A Fast Method for Visual Quality Prediction and Providing in Image Lossy Compression by SPIHT. Integrated Computer Technologies in Mechanical Engineering – 2020. Cham: Springer International Publishing, 17–29. https://doi.org/10.1007/978-3-030-66717-7_2
62. Li, F., Krivenko, S., Lukin, V. (2020). Adaptive two-step procedure of providing desired visual quality of compressed image. Proceedings of the 2020 4th International Conference on Electronic Information Technology and Computer Engineering. Xiamen, 407–414. https://doi.org/10.1145/3443467.3443791
63. Li, F., Krivenko, S., Lukin, V. (2020). An Approach to Better Portable Graphics (BPG) Compression with Providing a Desired Quality. 2020 IEEE 2nd International Conference on Advanced Trends in Information Theory (ATIT), 13–17. https://doi.org/10.1109/atit50783.2020.9349289
64. Li, F., Lukin, V. V., Okarma, K., Fu, Y., Duan, J.; Chen, C.-H. (Ed.) (2022). Intelligent Lossy Compression Method of Providing a Desired Visual Quality for Images of Different Complexity. Applied Mathematics, Modeling and Computer Simulation. IOS Press. https://doi.org/10.3233/atde220050
65. Li, F., Abramov, S., Dohtiev, I., Lukin, V. (2024). Advantages and drawbacks of two-step approach to providing desired parameters in lossy image compression. Advanced Information Systems, 8 (1), 57–63. https://doi.org/10.20998/2522-9052.2024.1.07
66. Li, F., Krivenko, S., Lukin, V. (2020). A Two-step Approach to Providing a Desired Visual Quality in Image Lossy Compression. 2020 IEEE 15th International Conference on Advanced Trends in Radioelectronics, Telecommunications and Computer Engineering (TCSET). Lviv-Slavske: IEEE, 502–506. https://doi.org/10.1109/tcset49122.2020.235483
67. Li, F., Krivenko, S., Lukin, V. (2020). Two-step providing of desired quality in lossy image compression by SPIHT. Radioelectronic and Computer Systems, 2, 22–32. https://doi.org/10.32620/reks.2020.2.02
68. Kozhemiakin, R., Lukin, V., Vozel, B. (2017). Image quality prediction for DCT-based compression. 2017 14th International Conference the Experience

of Designing and Application of CAD Systems in Microelectronics (CADSM). Lviv-Polyana: IEEE 225–228. https://doi.org/10.1109/cadsm.2017.7916121
69. Vozel, B., Kozhemiakin, R. A., Abramov, S. K., Lukin, V. V., Chehdi, K.; Bruzzone, L., Bovolo, F., Benediktsson, J. A. (Eds.) (2017). Output MSE and PSNR prediction in DCT-based lossy compression of remote sensing images. Image and Signal Processing for Remote Sensing XXIII. Warsaw: SPIE, 84. https://doi.org/10.1117/12.2278002
70. Krivenko, S., Zriakhov, M., Lukin, V., Vozel, B. (2018). MSE prediction in DCT-based lossy compression of noise-free and noisy remote sensing. 2018 14th International Conference on Advanced Trends in Radioelecrtronics, Telecommunications and Computer Engineering (TCSET). Lviv-Slavske: IEEE, 883–888. https://doi.org/10.1109/tcset.2018.8336338
71. Minguillo'n, J., Pujol, J. (2001). JPEG standard uniform quantization error modeling with applications to sequential and progressive operation modes. Journal of Electronic Imaging, 10 (2), 475–485. https://doi.org/10.1117/1.1344592
72. Abramova, V., Lukin, V., Abramov, S., Kryvenko, S., Lech, P., Okarma, K. (2023). A Fast and Accurate Prediction of Distortions in DCT-Based Lossy Image Compression. Electronics, 12 (11), 2347. https://doi.org/10.3390/electronics12112347
73. Abramova, V., Lukin, V., Abramov, S., Abramov, K., Bataeva, E. (2022). Analysis of Statistical and Spatial Spectral Characteristics of Distortions in Lossy Image Compression. 2022 IEEE 2nd Ukrainian Microwave Week (UkrMW). Kharkiv, 644–649. https://doi.org/10.1109/ukrmw58013.2022.10036949
74. Li, F., Kryvenko, S., Lukin, V.; Urbach, H. P., Jiang, H. (Eds.) (2023). Remote Sensing Image Lossy Compression Based on JPEG with Controlled Visual Quality. Proceedings of the 7th International Symposium of Space Optical Instruments and Applications. Singapore: Springer, 8–19. https://doi.org/10.1007/978-981-99-4098-1_2
75. Bondžulić, B., Stojanović, N., Petrović, V., Pavlović, B., Miličević, Z. (2021). Efficient Prediction of the First Just Noticeable Difference Point for JPEG Compressed Images. Acta Polytechnica Hungarica, 18 (8), 201–220. https://doi.org/10.12700/aph.18.8.2021.8.11
76. Lin, H., Chen, G., Jenadeleh, M., Hosu, V., Reips, U.-D., Hamzaoui, R., Saupe, D. (2022). Large-Scale Crowdsourced Subjective Assessment of Picturewise Just Noticeable Difference. IEEE Transactions on Circuits and Systems for Video Technology, 32 (9), 5859–5873. https://doi.org/10.1109/tcsvt.2022.3163860
77. Li, F., Lukin, V., Kryvenko, S., Bondzulic, B., Bujakovic, D., Pavlovic, B. (2023). Strange Images in Remote Sensing and Their Properties. Ukrainian Journal of Remote Sensing, 10 (2), 12–18. https://doi.org/10.36023/ujrs.2023.10.2.240

78. Pavlović, B., Bondžulić, B., Stojanović, N., Petrović, V., Bujaković, D. (2023). Prediction of the First Just Noticeable Difference Point based on Simple Image Features. 2023 Zooming Innovation in Consumer Technologies Conference (ZINC). Novi Sad, 125–130. https://doi.org/10.1109/zinc58345.2023.10173865
79. Bondžulić, B., Stojanović, N., Lukin, V., Stankevich, S. A., Bujaković, D., Kryvenko, S. (2024). Target acquisition performance in the presence of JPEG image compression. Defence Technology, 33, 30–41. https://doi.org/10.1016/j.dt.2023.12.006
80. Bondžulić, B., Pavlović, B., Stojanović, N., Petrović, V. (2022). Picture-wise just noticeable difference prediction model for JPEG image quality assessment. Vojnotehnicki Glasnik, 70 (1), 62–86. https://doi.org/10.5937/vojtehg70-34739